Covalent Bonding in $Au(BO)_2^-$ and $Au(BS)_2^-$

Chang-Qing Miao, Hai-Gang Lu & Si-Dian Li

Journal of Cluster Science
Including Nanoclusters and Nanoparticles

ISSN 1040-7278

J Clust Sci
DOI 10.1007/s10876-012-0546-z

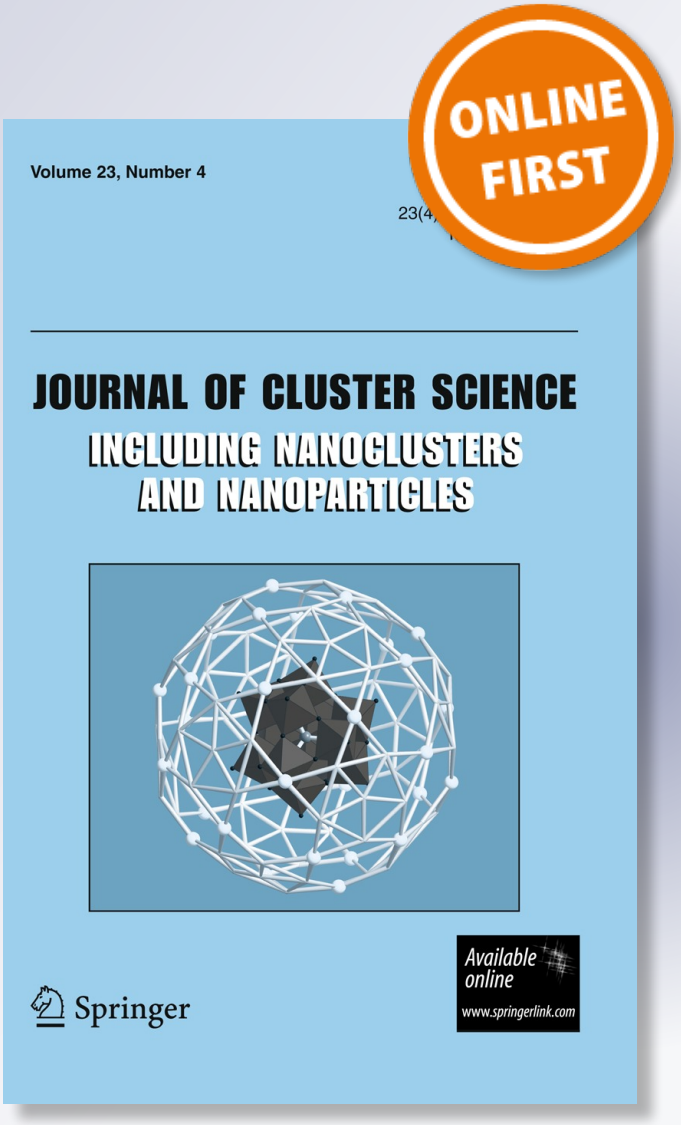

Springer

J Clust Sci
DOI 10.1007/s10876-012-0546-z

ORIGINAL PAPER

Covalent Bonding in $Au(BO)_2^-$ and $Au(BS)_2^-$

Chang-Qing Miao · Hai-Gang Lu · Si-Dian Li

Received: 11 July 2012

Abstract We perform in this work a comprehensive first-principles investigation on the geometric and electronic structures of $Au(BO)_2^-$ and $Au(BS)_2^-$ which are valent isoelectronic to the well-known $Au(CN)_2^-$ monoanion. $Au(BO)_2^-$ and $Au(BS)_2^-$ complexes prove to possess linear ground-state structures similar to $Au(CN)_2^-$ and the BO^- and BS^- ligands in them are found to be coordinated terminally via boron atoms to gold centers which are weakly negatively charged. Au–B bonds in $Au(BO)_2^-$ and $Au(BS)_2^-$ appear to have higher Wiberg bond indices (0.79 and 0.80) and more covalent components (60 and 53 %) than the corresponding values of Au–C interaction in $Au(CN)_2^-$ (0.67 and 39 %, respectively) at the same theoretical levels. Their Au–B bifurcation values of the electronic localization function also turn out to be higher than Au–C. These results strongly suggest that the Au–B bonds in $Au(BO)_2^-$ and $Au(BS)_2^-$ with multiple-bond character possess stronger covalent characters than Au–C in $Au(CN)_2^-$.

Keywords Gold complex · Ab initio calculation · Natural bonding orbital · Covalent bonding

Introduction

Recently, the catalytic chemistry of Au(I) complexes has attracted considerable attention [1]. Many Au(I) complexes, such as AuCN [2], $Au(CN)_2^-$ [3], AuO^-,

C.-Q. Miao · H.-G. Lu (✉) · S.-D. Li (✉)
Key Laboratory of Chemical Biology and Molecular Engineering of the Education Ministry, Institute of Molecular Science, Shanxi University, Taiyuan 030006, Shanxi, People's Republic of China
e-mail: luhg@sxu.edu.cn

S.-D. Li
e-mail: lisidian@yahoo.com; lisidian@sxu.edu.cn

Published online: 01 January 2013

AuS^- [4], AuX_2^- (X = Cl, Br and I) [5], $YAuCN^-$ (Y = F, Cl, Br and I) [6], had been investigated using combined experimental and theoretical methods. Because of the relativistic effects of gold [7], these Au(I) complexes exhibit different bonding characters from Cu(I) and Ag(I) complexes [3, 8]. For instance, the Au–C bonds in the most stable Au(I) ion, $Au(CN)_2^-$, possess significant covalent bonding with multiple-bond character due to Au 6s–5d hybridization, while the Cu–C and Ag–C bonds are mainly ionic in $Cu(CN)_2^-$ and $Ag(CN)_2^-$ complexes [3].

As isoelectronic ligand of CN^-, boronyl anion BO^- with a B≡O triple bond can form complexes with the transition metals [9–12], such as Au and Pt. Auro-boron oxides Au_nBO^- (n = 1–3) had been investigated by combined photoelectron spectroscopy and theoretical calculations [13], in which the Au_n cores were found to be terminated at a corner position by BO ligand through boron atom. Recently, Braunschweig et al. [14] synthesized for the first time the trans-$[(Cy_3P)_2BrPt(B{\equiv}O)]$ (Cy being cyclohexyl) crystal which contains a BO ligand with B≡O triple bond character.

As the valent isoelectronic complexes of $Au(CN)_2^-$, $Au(BO)_2^-$ and $Au(BS)_2^-$ monoanions may have similar geometric and electronic structures with $Au(CN)_2^-$. Because the Pauling electronegativity of boron (2.04) is lower than that of carbon (2.55), Au–B bond is expected to possess stronger covalent character than Au–C bond and a comparison between them would shed new insight into the bonding nature of Au(I) complexes in general. We present here a detailed first-principles investigation on the geometric and electronic structures and bonding characters of $Au(BO)_2^-$ and $Au(BS)_2^-$ and compare them with $Au(CN)_2^-$ throughout the work.

Computational Methods

We employed the Coalescence Kick (CK) global minimum search program [15, 16] to determinate the global minima of $Au(BO)_2^-$ and $Au(BS)_2^-$ on their potential energy surfaces, using the hybridized B3LYP [17, 18] method with the LanL2DZ basis [19] on gold and 3–21G on B, O, and S. All low-lying isomers found were re-optimized at the B3LYP level, with additional single-point calculations at the coupled cluster method including triple excitations (CCSD(T)) level [20–24], using the Stuttgart relativistic small-core pseudopotential and valence basis set augmented with two f and one g function on gold (SDD hereafter) [25] and aug-cc-pVTZ on the other elements (AVTZ hereafter) [26, 27]. The ground-state structures of linear $Au(BO)_2^-$, $Au(BS)_2^-$, and $Au(CN)_2^-$ were finally optimized at the CCSD(T)/SDD + AVTZ level. All calculations were performed using the Gaussian 09 package [28].

Chemical bonding was investigated by means of molecular orbital (MO), natural bond orbital (NBO 3.1) [29], and the quantum theory of atoms in molecules (QTAIM) [30] at the B3LYP/SDD + AVTZ level. Electron localization function (ELF) [31, 32] analysis was performed with the TOPMOD package [33] and the Jmol program [34] was chosen for the visualization of MO and ELF results. The QTAIM bond critical points and the total energy density of Au–B/C bonds were

obtained using PROAIM [35], and the QTAIM delocalization indices (bond orders) between Au and B/C atoms were evaluated using AIMDELOC [36].

Results and Discussion

Geometrical Structures

The reliability of our theoretical approach was first tested with $Au(CN)_2^-$ which possesses the calculated Au–C bond lengths of 2.01 and 2.05 Å at B3LYP/SDD + AVTZ and CCSD(T)/SDD + AVTZ (see Table 1), respectively. These values agree with the experimentally measured Au–C distances in solid $Au(CN)_2^-$ salts (1.98–2.12Å) and are well inline with the previous reported value of 1.99 Å obtained at PW91/TZ2P [3].

$Au(BO)_2^-$ and $Au(BS)_2^-$ anions turned out to possess singlet linear ground-state structures which lie much lower (>30 kcal/mol) than other isomers obtained at both B3LYP/SDD + AVTZ and CCSD(T)/SDD + AVTZ//B3LYP/SDD + AVTZ levels (Fig. 1). Furthermore, their triplet energies appeared to be about 106.5 and 82.4 kcal/mol higher than the singlet ones, respectively. The dissociation energies of $Au(BY)_2^- \rightarrow Au + BY^- + BY$ (Y = O or S) are more than 140 kcal/mol (Table 1), indicating that both the $Au(BO)_2^-$ and $Au(BS)_2^-$ complexes are highly stable.

In $Au(BO)_2^-$ and $Au(BS)_2^-$ anions, both BO^- and BS^- ligands are coordinated terminally via boron to the gold centers, similar to the CN^- ligand in $Au(CN)_2^-$. The calculated Au–B bond lengths of $r_{Au-B} = 2.10$ at B3LYP and $r_{Au-B} = 2.15$ Å at CCSD(T) are close to the Au–B single bond length of 2.09 Å [37], indicating that Au–B bond is approximately a single bond.

Because of their valent isoelectronic character and the geometric similarity with $Au(CN)_2^-$, $Au(BO)_2^-$ and $Au(BS)_2^-$ may serve as new candidate monoanions in gold catalytic chemistry. Such monoanions may be effectively stabilized in inorganic salts when incorporated with suitable counter-ions like Li^+ [11].

Table 1 Calculated bond lengths (r/Å) of the linear $Au(CN)_2^-$, $Au(BO)_2^-$ and $Au(BS)_2^-$ and dissociation energies (ΔE/(kcal/mol)) of $Au(BY)_2^- \rightarrow Au + BY^- + BY$ (Y = O or S) at the B3LYP and CCSD(T) levels using the SDD + AVTZ basis set

$Au(XY)_2^-$	Method	r_{Au-X}	r_{X-Y}	ΔE
$Au(CN)_2^-$	B3LYP	2.01	1.16	
	CCSD(T)	2.05	1.14	
	PW91/TZ2P[a]	1.99	1.17	
$Au(BO)_2^-$	B3LYP	2.10	1.22	171.7
	CCSD(T)	2.15	1.20	143.8
$Au(BS)_2^-$	B3LYP	2.09	1.65	167.4
	CCSD(T)	2.14	1.64	232.3

[a] Ref. 3

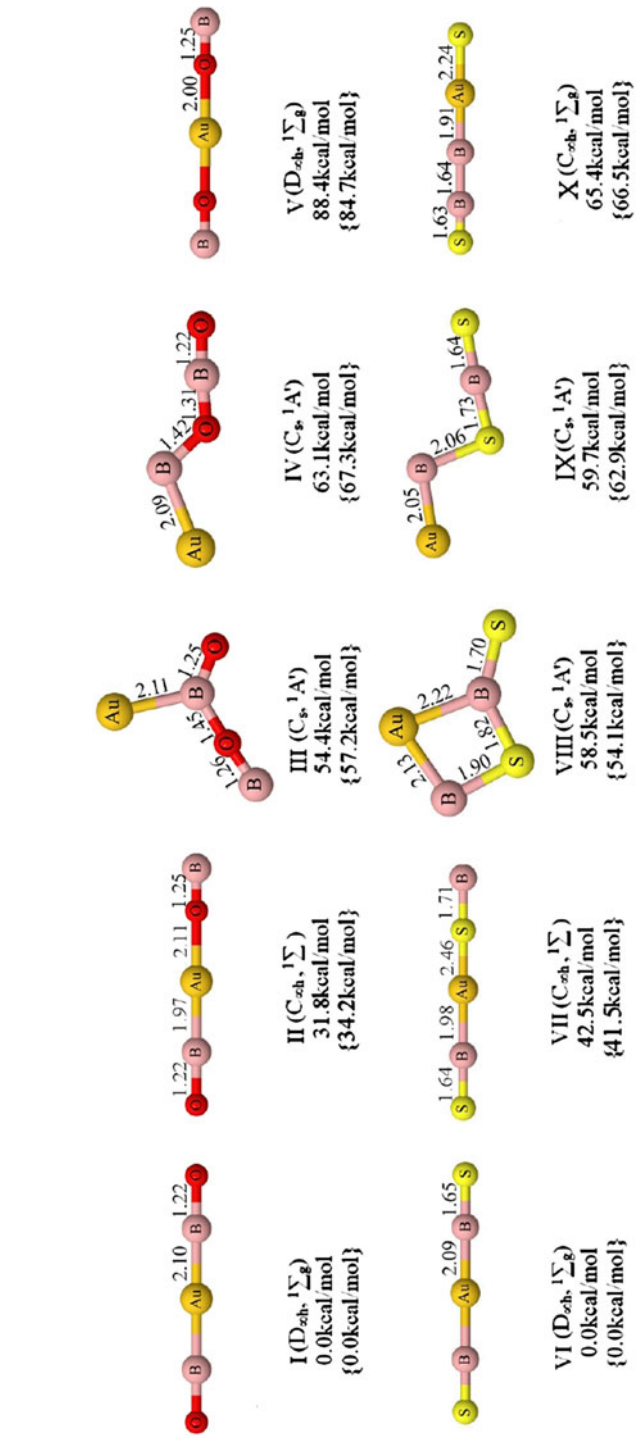

Fig. 1 Optimized isomers of $Au(BO)_2^-$ (I–V) and $Au(BS)_2^-$ (VI–X) with bond lengths indicated in Å. Relative energies (including the thermal correction) are given at B3LYP/SDD + AVTZ and CCSD(T)/SDD + AVTZ//B3LYP/SDD + AVTZ (in *curly brackets*)

Covalent Bonding Character

Because the relativistic effects stabilize Au 6s orbital and destabilize Au 5d orbitals to reduce the 6s–5d energy gap and enhance s-d hybridization, Au exhibits significant covalent bonding characters, in contrast to its lighter congeners Ag and Cu. For instance, Au–C forms significant covalent Au–C bond with multiple-bond character, as observed in $Au(CN)_2^-$ [3, 8].

Similar covalent bonding occurs to $Au(BO)_2^-$ and $Au(BS)_2^-$. As shown in Table 2, the calculated net natural atomic charge of Au is +0.20, −0.20 and −0.05 |el| in $Au(CN)_2^-$, $Au(BO)_2^-$ and $Au(BS)_2^-$, respectively, which indicates that gold acts as a weak electron donor in $Au(CN)_2^-$ and weak electron acceptors in both $Au(BO)_2^-$ and $Au(BS)_2^-$ due to the difference in electronegativiy between boron and carbon. The Au–B Wiberg bond indices [38] are 0.79 and 0.80 in $Au(BO)_2^-$ and $Au(BS)_2^-$, respectively, which are obviously higher than corresponding value of 0.67 obtained for Au–C in $Au(CN)_2^-$ at the same theoretical level. More interestingly, the covalent components of 60 and 53 % calculated for the Au–B bonds in $Au(BO)_2^-$ and $Au(BS)_2^-$ at natural resonance theory (NRT) are obviously higher than the covalent component of 39 % obtained for Au–C bond in $Au(CN)_2^-$. The triple bonds in C ≡ N, B ≡ O, and B ≡ S ligands are also well demonstrated by their calculated NRT bond orders between $NRT_{X\text{-}Y} = 2.98 \sim 2.96$ (see Table 2). These results strongly suggest that the Au–B bonds in $Au(BO)_2^-$ and $Au(BS)_2^-$ (which are mainly covalent as indicated above) possess stronger covalent bond character than the Au–C bonding observed in $Au(CN)_2^-$ [3, 8].

Electron localization functions (ELF) reflecting the probability to find electron pairs in specific regions provide a more vivid description of the increasing covalence from Au–C to Au–B (see Fig. 2). The ELF bifurcation values [30, 31] estimated from ELF pictures increase from 0.25 in $Au(CN)_2^-$ to 0.30 in both $Au(BO)_2^-$ and $Au(BS)_2^-$ (see Table 2). These values provide further evidences to support the increasing covalence from $Au(CN)_2^-$ to $Au(BO)_2^-$ and $Au(BS)_2^-$.

The negative value of the total energy density (H_{bcp}) at the bond critical point (BCP) is an alterative indictor of covalent bond [39]. The negative H_{bcp}'s values calculated for these three gold complexes (Table 2) indicate that the Au–X (X = C,

Table 2 Natural atomic charges (Q/|el|), Wiberg bond indices (WBI), NRT bond orders (NRT) and their covalent component percentages (CNRT) and ionic component percentages (INRT), the bifurcation values of electronic localization functions (ELF), and the total energy densities at QTAIM bond critical points (H_{bcp}) of Au–B/C bonds obtained for $Au(CN)_2^-$, $Au(BO)_2^-$, and $Au(BS)_2^-$

$Au(XY)_2^-$	Q_{Au}	Q_x	Q_y	WBI	NRT	CNRT (%)	INRT (%)	NRT_{X-Y}	ELF	H_{bcp}
$Au(CN)_2^-$	0.20	−0.07	−0.53	0.67[a]	0.93	39	61	2.98	0.25	−0.06
$Au(BO)_2^-$	−0.20	0.53	−0.94	0.79	0.90	60	40	2.97	0.30	−0.07
$Au(BS)_2^-$	−0.05	−0.01	−0.47	0.80	0.92	53	47	2.96	0.30	−0.05

[a] With Au 6p explicitly included as valence atomic orbitals in NBO analyses in the Gaussian 09 package employed in this work. Using NBO analysis in Gaussian03 package, the calculated WBI_{Au-C} value of 0.55 is very close to that of $WBI_{Au-C} = 0.58$ reported in Ref. 3

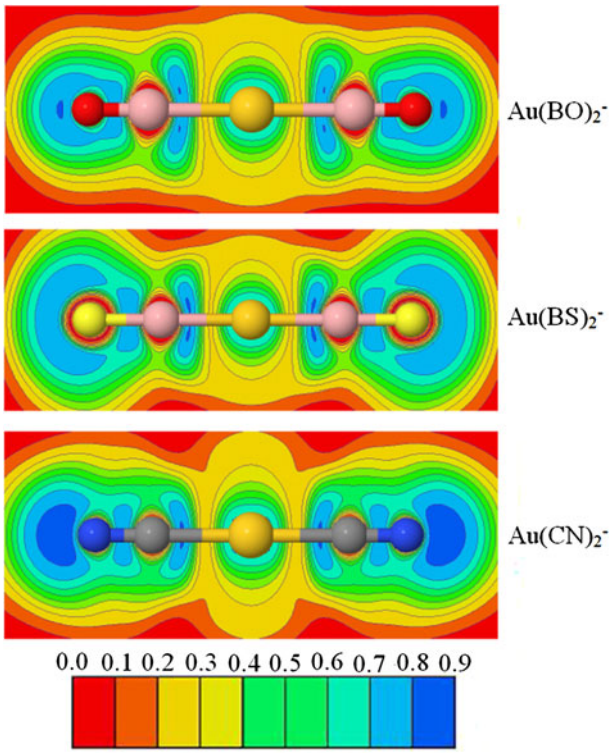

Fig. 2 ELFs for $Au(BO)_2^-$, $Au(BS)_2^-$ and $Au(CN)_2^-$

B) bonds in them possess obvious covalent character. However, their magnitudes are small, suggesting that the covalent character of these bonds is relatively weak.

Molecular Orbital Analysis

Canonical molecular orbital pictures show the Au–X bonding patterns of $Au(CN)_2^-$, $Au(BO)_2^-$, and $Au(BS)_2^-$. As shown in Fig. 3a for $Au(BO)_2^-$, the HOMO (σ_u) and HOMO-8 (σ_g) mainly stand for the most concerned Au–B σ interactions (with HOMO-6 (σ_g) also making certain contribution to Au–B bonding). The doubly degenerate HOMO-5 and HOMO-2 represent the Au–B π bonding and π* antibonding, respectively (which will cancel each other in principle). The other valence MOs stand for the B≡O triple bonds (two πMOs and one σ MO) and the non-bonding lone pairs on Au or oxygen atoms. The bonding picture of $Au(BS)_2^-$ is very similar to that of $Au(BO)_2^-$, except for the slight difference in MO energy order (Fig. 3b).

Detailed natural bond orbital analysis help to reveal the subtle differences between Au–B and Au–C bonds. Natural population analysis indicate that the valence orbital populations of Au are $6s^{1.03}5d^{9.64}6p_z^{0.14}$, $6s^{1.23}5d^{9.74}6p_z^{0.24}$ and $6s^{1.12}5d^{9.72}6p_z^{0.22}$ in $Au(CN)_2^-$, $Au(BO)_2^-$ and $Au(BS)_2^-$, respectively. The increasing

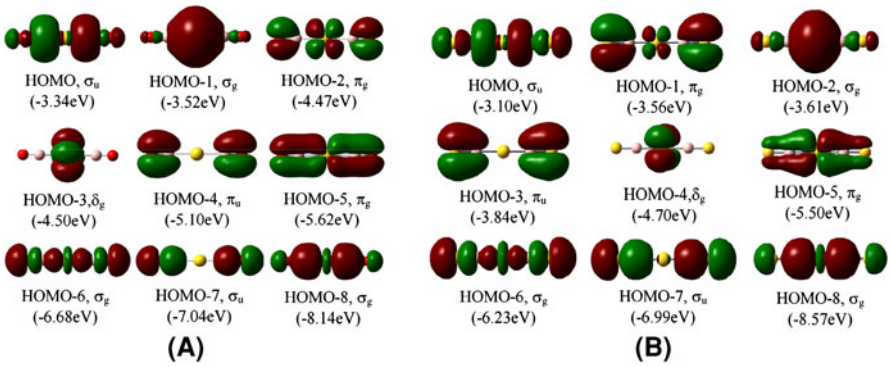

Fig. 3 Canonical molecular orbitals (with an isovalue of 0.02 a.u.) and their energies (in *brackets*) of linear $Au(BO)_2^-$ (**a**) and $Au(BS)_2^-$ (**b**) at B3LYP/SDD + AVTZ level. All the π and δ MOs are doubly degenerate in energy

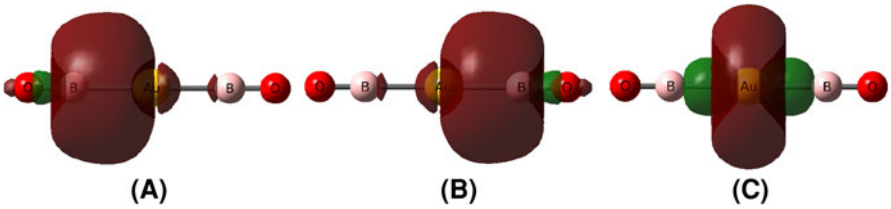

Fig. 4 NRT bonding orbitals of $Au(BO)_2^-$ with an isovalue of 0.02 a.u. at B3LYP/SDD + AVTZ level: **a** and **b** are the Au–B σ orbitals and **c** is the Au s–d_{z^2} hybridization orbital

$6p_z$ populations (0.14–0.24) indicate that Au 6p orbitals play an important role in the formation of the Au–B/C bonds and they should be included as valence atomic orbitals in theoretical calculations (as we did in this work). The atomic orbital populations of Au in $Au(BO)_2^-$ and $Au(BS)_2^-$ are about 0.08–0.20 |e| higher than that in $Au(CN)_2^-$ which are in good agreement with the net atomic charges Au carries in theses monoanions (see Table 2). Thus, every Au valence orbital makes certain contribution to promote the covalent components in Au–B bonds compared to Au–C bond.

NRT bond orbital analysis indicates that there are two equivalent Au–C or Au–B σ bonds linearly arranged around the Au center (Fig. 4a and b), with the orbital hybridizations of 0.45Au $sp^{1.24}$ + 0.89C $sp^{0.85}$, 0.55Au $sp^{1.19}$ + 0.83B $sp^{0.60}$, and 0.53Au $sp^{1.14}$ + 0.85B $sp^{0.81}$ for $Au(CN)_2^-$, $Au(BO)_2^-$, and $Au(BS)_2^-$, respectively. Au $sp^{1.14-1.24}$ hybridized atomic orbitals contribute 20, 30, and 28 % to the Au–X σ bonds in $Au(CN)_2^-$, $Au(BO)_2^-$, and $Au(BS)_2^-$, respectively (Note the important contributions from Au 6p as mentioned above). Such an increasing percentage enhances the covalence of the Au-X bonds from Au–C to Au–B. In addition, there is an s–d_{z^2} hybridization lone-pair orbital on the Au center which reaches the vicinity of B/C atoms (Fig. 4c). Although there is no explicit overlap between Au s–d_{z^2} and B/C, the extended Au s–d_{z^2} orbital is expected to make certain contribution to Au–B/C

bonding, rendering multiple-bond character to the Au-X bonds in $Au(CN)_2^-$, $Au(BO)_2^-$, and $Au(BS)_2^-$.

To quantitatively describe the multiple-bond character of Au–B bonds, the numbers of electron pairs shared between Au and B atoms were evaluated using the QTAIM delocalization index by integrating the exchange density once over each of the two atomic basins. [40] The Au–X shared electron pairs are 1.00, 1.11, and 1.09 in the $Au(CN)_2^-$, $Au(BO)_2^-$, and $Au(BS)_2^-$, respectively. Obviously, the Au–B bond orders are greater than one and therefore the Au–B interactions in both $Au(BO)_2^-$ and $Au(BS)_2^-$ possess certian multiple bond character.

Conclusion

In conclusion, we reported an ab initio study on the Au(I) complexes: $Au(BO)_2^-$ and $Au(BS)_2^-$. Their geometric structures are linear and the BO and BS ligands in them are coordinated terminally via boron to the metal center, similar to the situation in $Au(CN)_2^-$. The calculated Wiberg bond indices, covalent component percentages, and ELF bifurcation values of Au–B bonds appear to be higher than that of the Au–C bond, suggesting that the Au–B bonds in $Au(BO)_2^-$ and $Au(BS)_2^-$ possess stronger covalent bond characters than Au–C bonding in $Au(CN)_2^-$. Furthermore, the natural bond orbital analysis and the QTAIM shared electron pairs demonstrated that the Au–B bonds possess multiple bond character in $Au(BO)_2^-$ and $Au(BS)_2^-$. As Auro-boron oxides Au_nBO^- ($n = 1$–3) have been observed in experiments, their analogues of $Au(BO)_2^-$ and $Au(BS)_2^-$ are expected to be synthesized in gas phases by laser ablation and characterized with photoelectron spectroscopy measurements combined with ab initio calculations.

Acknowledgments This work was jointly supported by the National Natural Science Foundation of China (Grant No. 20873117) and Shanxi Science Foundation (No. 2010011012-3). SDL sincerely thanks Prof. Jun Li at Tsinghua University for inspiration discussions on the project.

References

1. D. J. Gorin and F. D. Toste (2007). *Nature* **446**, 395.
2. T. Okabayashi, E. Y. Okabayashi, F. Koto, T. Ishida, and M. Tanimoto (2009). *J. Am. Chem. Soc.* **131**, 11712.
3. X.-B. Wang, Y.-L. Wang, J. Yang, X.-P. Xing, J. Li, and L.-S. Wang (2009). *J. Am. Chem. Soc.* **131**, 16368.
4. H.-J. Zhai, C. Bürgel, V. Bonacic-Koutecky, and L.-S. Wang (2008). *J. Am. Chem. Soc.* **130**, 9156.
5. D. Schröder, R. Brown, P. Schwerdtfeger, X.-B. Wang, X. Yang, L.-S. Wang, and H. Schwarz (2003). *Angew. Chem. Int. Ed.* **42**, 311.
6. H.-T. Liu, X.-G. Xiong, P. D. Dau, Y.-L. Wang, J. Li, and L.-S. Wang (2011). *Chem. Sci.* **2**, 2101.
7. P. Pyykkö (2004). *Angew. Chem. Int. Ed.* **43**, 4412.
8. L.-S. Wang (2010). *Phys. Chem. Chem. Phys.* **12**, 8694.
9. H.-J. Zhai, L.-M. Wang, S.-D. Li, and L.-S. Wang (2007). *J. Phys. Chem. A* **111**, 1030.
10. H.-J. Zhai, S.-D. Li, and L.-S. Wang (2007). *J. Am. Chem. Soc.* **129**, 9254.
11. S.-D. Li, H.-J. Zhai, and L.-S. Wang (2008). *J. Am. Chem. Soc.* **130**, 2573.
12. W.-Z. Yao, J.-C. Guo, H.-G. Lu, and S.-D. Li (2009). *J. Phys. Chem. A* **113**, 2561.
13. D Yu Zubarev and A. I. Boldyrev (2007). *J. Phys. Chem. A* **111**, 1648.

14. H. Braunschweig, K. Radacki, and A. Schneider (2010). *Science* **328**, 345.
15. X. Li, B. Kiran, J. Li, H.-J. Zhai, and L.-S. Wang (2002). *Angew. Chem. Int. Ed.* **41**, 4786.
16. B. B. Averkiev and Ph D Dissertation *Utah State University* (Logan, Utah, 2009).
17. A. D. Becke (1993). *J Chem. Phys.* **98**, 5648.
18. C. Lee, W. Yang, and R. G. Parr (1988). *Phys. Rev. B* **37**, 785.
19. P. J. Hay and W. R. Wadt (1985). *J. Chem. Phys.* **82**, 299.
20. J. Cizek (1969). *Adv. Chem. Phys.* **14**, 35.
21. G. D. Purvis III and R. J. Bartlett (1982). *J. Chem. Phys.* **76**, 1910.
22. G. E. Scuseria, C. L. Janssen, and H. F. Schaefer III (1988). *J. Chem. Phys.* **89**, 7382.
23. G. E. Scuseria and H. F. Schaefer III (1989). *J. Chem. Phys.* **90**, 3700.
24. J. A. Pople, M. Head-Gordon, and K. Raghavachari (1987). *J. Chem. Phys.* **87**, 5968.
25. M. Dolg, H. Stoll, H. Preuss, and R. M. Pitzer (1993). *J. Phys. Chem.* **97**, 5852.
26. T. H. Dunning Jr (1989). *J. Chem. Phys.* **90**, 1007.
27. D. E. Woon and T. H. Dunning Jr (1993). *J. Chem. Phys.* **98**, 1358.
28. M. J. Frisch, G. W. Trucks, and H. B. Schlegel, et al., *Gaussian 09, Revision, A.1* (Pittsburgh: Gaussian, Inc., 2009).
29. A. E. Reed, L. A. Curtiss, and F. Weinhold (1988). *Chem. Rev.* **88**, 899.
30. R. F. W. Bader *Atoms in molecules–a Quantum theory* (Oxford University Press, Oxford, 1990).
31. A. D. Becke and K. E. Edgecombe (1990). *J. Chem. Phys.* **92**, 5397.
32. A. Savin, J. Flad, H. Preuss, O. Jepsen, O. K. Andersen, and H. G. von Schnering (1992). *Angew. Chem.* **104**, 186.
33. S. Noury, X. Krokidis, F. Fuster, and B. Silvi *TOPMOD Package* (Universite Pierre et Marie Curie, Paris, 1997).
34. Jmol: an open-source Java viewer for chemical structures in 3D. http://www.jmol.org/.
35. R. F. W. Bader, AIMPAC. http://www.chemistry.mcmaster.ca/aimpac/.
36. C. F. Matta, AIMDELOC: Program to calculate AIM localization and delocalization indices. (http://www.chem.utoronto.ca/∼cmatta/).
37. P. Pyykkö and M. Atsumi (2009). *Chem. Eur. J.* **15**, 12770.
38. K. B. Wiberg (1968). *Tetrahedron* **24**, 1083.
39. D. Cremer and E. Kraka (1984). *Angew. Chem. Int. Ed.* **23**, 627–628.
40. X. Fradera, M. A. Austen, and R. F. W. Bader (1999). *J. Phys. Chem. A* **103**, 304.